



Enhanced radio-photodynamic therapy potential of advanced gold-based nanoclusters for breast cancer treatment

Omid Talaei¹ · Reza Faghihi^{1,2} · Banafsheh Rastegari³ · Sedigheh Sina^{1,2}

Received: 6 February 2024 / Revised: 31 May 2024 / Accepted: 23 June 2024 / Published online: 16 July 2024

© The Author(s), under exclusive licence to Japanese Society of Radiological Technology and Japan Society of Medical Physics 2024

Abstract

The purpose of current study was to assess the impact of ALA-coated gold nanoclusters (Au NPs) on the combined therapeutic effects of radiotherapy (RT) and photodynamic therapy (PDT) on healthy MCF-10A and MCF-7 breast cancer cells. The Au NPs were covered with ALA using PEG polymer, resulting in the synthesis of Au@ALA NPs. The successful synthesis of the final NPs was confirmed through FTIR, XRD, TEM, and UV–Vis tests. MCF-10A and MCF-7 cell lines were treated with different concentrations of Au@ALA NPs and exposed to irradiation of 2 and 4 Gy (using MV X-ray) and 630 nm laser light irradiation. Cytotoxicity was assessed using a multifaceted approach involving the MTT assay, real-time PCR, and colony forming assay. The findings revealed that the damage inflicted by Au@ALA NPs on cancerous tissue was significantly greater than that on normal tissue. The cytotoxic effects of all experimental groups exhibited a direct correlation with increasing concentrations and radiation doses. The combination of Au@ALA NPs with RT doses of 2 and 4 Gy resulted in a reduction in cell viability by a factor of 1.58 ($P=0.001$) and 1.73 ($P=0.004$), respectively. Furthermore, the simultaneous intervention of NPs with PDT and RT at doses of 2 and 4 Gy led to a decrease in cell viability by a factor of 2.10 ($P=0.001$) and 3.08 ($P=0.001$) in turn. Furthermore, the real-time PCR and colonogenic assay results demonstrated that the combined treatment significantly increased phosphorylation of ATM and expression of TP53, indicating an adequate synergistic effect on breast cancer cells. The concurrent application of Au@ALA NPs in RT and PDT successfully enhanced the radiosensitization of breast cancer cells to megavoltage RT and PDT.

Keywords Breast cancer · Radiation therapy · Photodynamic therapy · Nanocluster · Nanoparticle · Dose enhancement

1 Introduction

Breast cancer (BC) is a significant global health concern in women, leading to substantial mortality [1]. It is associated with unrestrained progress and metastasis to organs alike the liver, brain, and bone, occurring in 10% and 40% of early and advanced stages, respectively [2]. Currently, radiotherapy (RT) is employed in the treatment of over 80% of BC patients. In RT, the aim is to deliver an extraordinary

dose of radiation to the cancerous cells while minimizing damage to nearby healthy tissues [3].

The emergence of nanotechnology has opened new avenues for the diagnosis and treatment of cancer. Nanoparticles (NPs) with high atomic numbers have shown great promise in delivering therapeutic agents to cancer cells, thereby enhancing localized energy transfer to the tumor. NPs serve as effective carriers for drug delivery, improving targeted delivery to tumor cells [4]. Moreover, NPs offer additional advantages, such as modulating the cell cycle, generating reactive oxygen species (ROS), triggering inflammatory responses, causing harm to genetic material, and inducing cell death [5]. ROS can induce apoptosis in several cell cultures [6]. Furthermore, NPs have facilitated the development of therapeutic modalities like photodynamic therapy (PDT) [7], photothermal therapy (PTT) [8], sonodynamic therapy (SDT) [9], and even RT [10, 11].

A novel strategy to increase cancer cell death while maintaining the normal collateral tissues undamaged is

✉ Reza Faghihi
faghihir@shiraz.ac.ir

¹ Nuclear Engineering Department, Shiraz University, Shiraz, Iran

² Radiation Research Center, Shiraz University, Shiraz, Iran

³ Diagnostic Laboratory Sciences and Technology Research Center, School of Paramedical Sciences, Shiraz University of Medical Sciences, Shiraz, Iran

to target nanomaterial such as gold nanoparticles (Au NPs) by RT and PDT inside the cancerous cells. Studies revealed that the high atomic number of metal elements induces greater radiation damage to the target cells [12]. Recently, experiments demonstrated that Au NPs can serve as a radiosensitizer to increase the absorbed radiation dose due to the intensified probability of photoelectric effects because of its high atomic number ($Z=79$) [13]. The penetration of NPs into tumorous cells improves local energy transmitted to the tumor, grows radiation-induced destruction to the tumor, and reduces undesirable damage to adjacent healthy tissue [14].

Furthermore, PDT is also considered a promising approach in the treatment of cancer that uses a two-phase process of injecting a photosensitizer (PS) agent followed by exposure to light that generates toxicity to malignant cells [15]. The excitement of PSs by light absorption triggers the reaction with substrates to generate free radicals. The absorbed energy in the PSs can also be transferred to molecular triplet oxygen to generate ROS [16]. Among numerous PSs, 5-aminolevulinic acid (5-ALA) is widely used as an FDA-accepted PS pioneer in PTT with low toxicity and fast clearance (24–48 h) from the body [17, 18]. ALA is transformed into protoporphyrin IX (PpIX) in the mitochondrion after being internalized by cancer cells [19]. The advantage of the photosensitive fluorescent molecule of PpIX is its ability to degrade at diverse rates in normal and cancer cells [20].

The key goal in competing against tumors is finding operative therapeutic methods with high specificity and low toxicity to eradicate cancers and their metastases and prevent their recurrence. However, this relevant result is hard to achieve with the current approaches for cancer treatment, such as chemotherapy, surgery, and RT [21]. For example, radiation ionization does not distinguish the cancer cells from neighboring normal tissue, which causes early and late side effects that finally reduce the patient's quality of life [22]. Another limiting factor of RT is its cytotoxicity which prevents it from reaching the maximum RT dose [23]. One solution to these problems is increasing the therapeutic ratio of RT and PDT with the aid of NPs which helps to kill more cancerous cells while reducing damage to the neighboring normal tissue [5, 13, 17]. Another promising strategy is to use a therapeutic method along with another one to increase the efficacy of the treatment. Various modalities, such as PTT, gene therapy, and immunotherapy [24] or chemo-photothermal therapy [25], have been used in treating cancer simultaneously.

In this work, we examined the combined therapeutic influence of RT and PDT on MCF-7 BC cells after using a multifunctional nano-complex of targeted PEG-Au NPs coated with ALA. While the Au core serves to enhance RT efficiency, the ALA shell produces a strong PDT PSs' effect.

2 Materials and methods

2.1 Study design

The cells in this research are categorized into seven groups: (i) cells without any intervention (without Au@ALA NPs, laser, or MV radiation), (ii) cells treated with Au@ALA NPs, (iii) empty cells with laser radiation, (iv) treated cells (with Au@ALA NPs) and laser radiation, (v) empty cells with MV radiation, (vi) treated cells (with Au@ALA NPs) and MV radiation, and finally (vii) treated cells (with Au@ALA NPs) and laser + MV radiation.

2.2 Material

Ammonia solution (25%), perchloric acid (HClO_4 , 70–72%), 1,4-dioxane, dimethyl sulfoxide (DMSO), sodium citrate dehydrates, ammonia solution (25–28%), and HAuCl_4 were procured from Merck Chemicals. Polyethylene glycol (PEG) with a molecular weight of 2 kDa was taken from Iris Biotech GmbH, Marktredwitz, Germany, and used as received. The human breast adenocarcinoma (MCF-7) and normal breast (MCF-10A) cell lines were acquired from the Pasteur Institute of Iran. Distilled water was used throughout the tests.

2.3 Preparing Au@ALA NPs

We employed the citrate chemical reduction method, as described by Anshup et al. [26], to synthesize Au NPs. Here, 0.01 g of Au salt (HAuCl_4) was dissolved in 5 mg of deionized water. The resulting Au salt solution was combined with 90 ml of water and located on a magnetic stirrer. Upon boiling the solution, sodium citrate was added. It caused a color change in the solution from pale yellow to dark red, indicating the synthesis of Au NPs. The synthesized NPs were filtered using a 0.22 μm filter paper and purified through centrifugation. To become stable with the manufactured Au NPs, 0.1 ml of a 3% w/v polyethylene glycol (PEG) solution was added to 10 ml of the Au NPs solution and stirred on a magnetic stirrer for 4 h. To conjugate the Au NPs with the 5-ALA drug, we initially dissolved 25 μl of the 5-ALA drug (manufactured by Merck) in water and added it to 10 ml of the Au NPs solution. The mixture was then stirred for 4 h using a magnetic stirrer.

2.4 Nanoparticles characterization

The sizes and shapes of the Au NPs were concluded with transmission electron microscopy (TEM) and scanning electron microscopy (SEM), and their analysis was performed using

Image J software. Fourier transform infrared spectroscopy (FTIR) spectra were achieved using a Shimadzu Prestige-21 spectrometer (Shimadzu Corp., Kyoto, JP) with a resolution of 2 cm^{-1} in the range of 4000 cm^{-1} to 400 cm^{-1} . X-ray diffraction (XRD) was engaged to determine the structural characteristics of the Au@ALA NPs. This measurement was conducted using a Bruker D8 Advance 3 kW diffractometer with a copper radiation tube. The correct synthesis of the Au@ALA NPs was confirmed using ultraviolet–visible (UV–Vis) spectroscopy, performed on a JASCO spectrophotometer (Model V-570, JASCO Inc., Japan). Additionally, the hydrodynamic diameters and zeta potential of the Au@ALA NPs were evaluated using dynamic light scattering (DLS) with a Nano Zeta-Sizer (DTS1060, Malvern Instruments, Malvern, UK).

2.5 Cell culture

Cells were kept in sterile flasks in the Dulbecco's Modified Eagle Medium (DMEM) containing 10% Fetal Bovine Serum (FBS) and the antibiotics penicillin and streptomycin. The cells were cultivated and multiplied in an incubator at $37\text{ }^{\circ}\text{C}$ and 5% carbon dioxide. After several passages of cells, when they reached exponential growth, they were separated from the bottom of the flask by trypsin–EDTA. After counting the cells, the percentage of living cells was determined using trypan blue and Nicobar lam. Then, the appropriate number of cells was poured into each well of the 96-well plate to perform the desired tests. Cells were divided into five experimental groups. (i) control group (without any interventions), (ii) NPs group (cells with Au@ALA NPs), (iii) radiotherapy group (cells with Au@ALA NPs + treated with 2 and 4 Gy radiotherapy), (iv) PDT group (cells with Au@ALA NPs and PDT), and (v) combined treatment group (cells with Au@ALA NPs + radiotherapy + PDT).

2.6 Cell viability

The MTT method is a simple and rapid approach to assess cell viability. It relies on the reduction of MTT or other tetrazolium salts, leading to the formation of formazan color. Within living cells, the tetrazolium ring of MTT is cleaved by mitochondrial enzymes, resulting in the formation of insoluble purple formazan quartzes. The presence of these crystals specifies the movement of respiratory chain enzymes and serves as an indicator of cell viability. The absorbance at specific wavelengths can be measured to control the number of viable cells. The percentage of living cells or the cell survival rate can be calculated using the following equation:

$$\% \text{ Cell viability} = 100 \times \text{Experimental well absorbance} / \text{untreated control well absorbance.} \quad (1)$$

Here, cells were poured in the appropriate concentration into 96-well plates for each test. The survival of the cells is measured by the MTT after performing the tests related to each group. In this method, 0.5 mg/ml of MTT was furthered to each well-containing cell, and after 4 h, the cell sedimentations were carried out in dimethyl sulfoxide (DMSO) and glycine buffer. The optical absorption of formazan crystals was measured by the ELISA device at a wavelength of 540 nm, and the viability of the cells of each sample was designed in contrast with the control group [13].

2.7 Cell irradiation

The examples were exposed to absorbed doses of 2 Gy and 4 Gy using radiation beams of 6 MV from a Siemens ONCOR Linear Accelerator (Siemens AG, Henkestr, Erlangen, Germany). To ensure uniform exposure, the cell plates were occupied with water and positioned around the treated cell plate, creating a fully scattered background. The field size was set to $16 \times 12\text{ cm}^2$, and the source–axis distance (SAD) was maintained at 100 cm. Additionally, the samples were located on a 5 cm slab of polystyrene at the center of the beam, providing adequate buildup for sufficient backscatter. After radiation, the treated and control cells were immediately returned to the incubator.

For the treatment groups using low-power NIR laser (630 nm , 590 mW/cm^2), the cancer cells were irradiated. Initially, the MCF-10 and MCF-7 cell lines, with a cell density of 1.5×10^4 in each well, were subjected to treatment with different concentrations of Au@ALA NPs. Subsequently, the laser light was applied to the cells for 5 min.

2.8 Real-time PCR (qRT-PCR)

The total cellular RNA was isolated from MCF-7 and MCF-10 cell lines using Trizol reagent (RiboEX-GeneAll). Yekta Tajhiz (Yekta Tajhiz, Tehran, Iran) cDNA synthesis kit was utilized to generate cDNA. Subsequently, the qRT-PCR was performed to assess the expression levels of *TP53* and *ATM* using SYBR Green Master Mix (Ampliqon, Denmark). *GAPDH* was utilized as an internal control for normalizing the expression ratio of genes, and the findings were analyzed by the $2^{-\Delta\Delta\text{CT}}$ method.

2.9 Colony formation assay (CFA)

CFA was performed to investigate the inhibitory effect of X-ray, Laser, Au@ALA NPs, and X-ray + laser + Au@ALA NPs groups on the colony formation capacity of MCF-7 breast cancer cells. A total of 4×10^3 of the cells were seeded into a 6-well plate and after treatments cultured for 3 days. Afterward, the cells were washed with PBS fixed with 5% paraformaldehyde and stained with 0.5% crystal violet for 30 min. Finally, the plates were washed with water and colonies were pictured using an inverted microscope.

2.10 Statistical analysis

The experiments were meticulously carried out, ensuring a minimum of three independent replicates for each test. The results obtained were presented as the mean \pm standard deviation (SD), which provides a measure of the data's dispersion. To evaluate the differences between groups, statistical analyses were conducted using both Student's *t* test and Wilcoxon analysis, with a confidence interval of 95%. For the statistical analyses, the data were processed using SPSS

22.0 software (SPSS, Inc., Armonk, NY, USA), which is a widely recognized tool for statistical analysis in the scientific community. A *p* value of less than 0.05 was considered to be statistically significant. In the presented results, asterisks were used to indicate the level of significance, with * representing $P < 0.05$ and ** representing $P < 0.01$.

3 Results

3.1 Characterization of Au@ALA NPs

Schematic synthesis steps of the novel NPs with surface reform with ALA are offered in Fig. 1A. First, the Au NPs were synthesized using HAuCl_4 with sodium citrate. Secondly, after coating Au NPs with PEG, the ALA conjugated to the Au NPs for increased stability and bio-compatibility. Not only with PEGylating, the human body does not consider the NPs as external substances but also the target drugs can be labeled on the NPs.

Figure 1B displays the X-ray diffraction (XRD) analysis of Au@ALA NPs. The XRD pattern exhibits four distinct

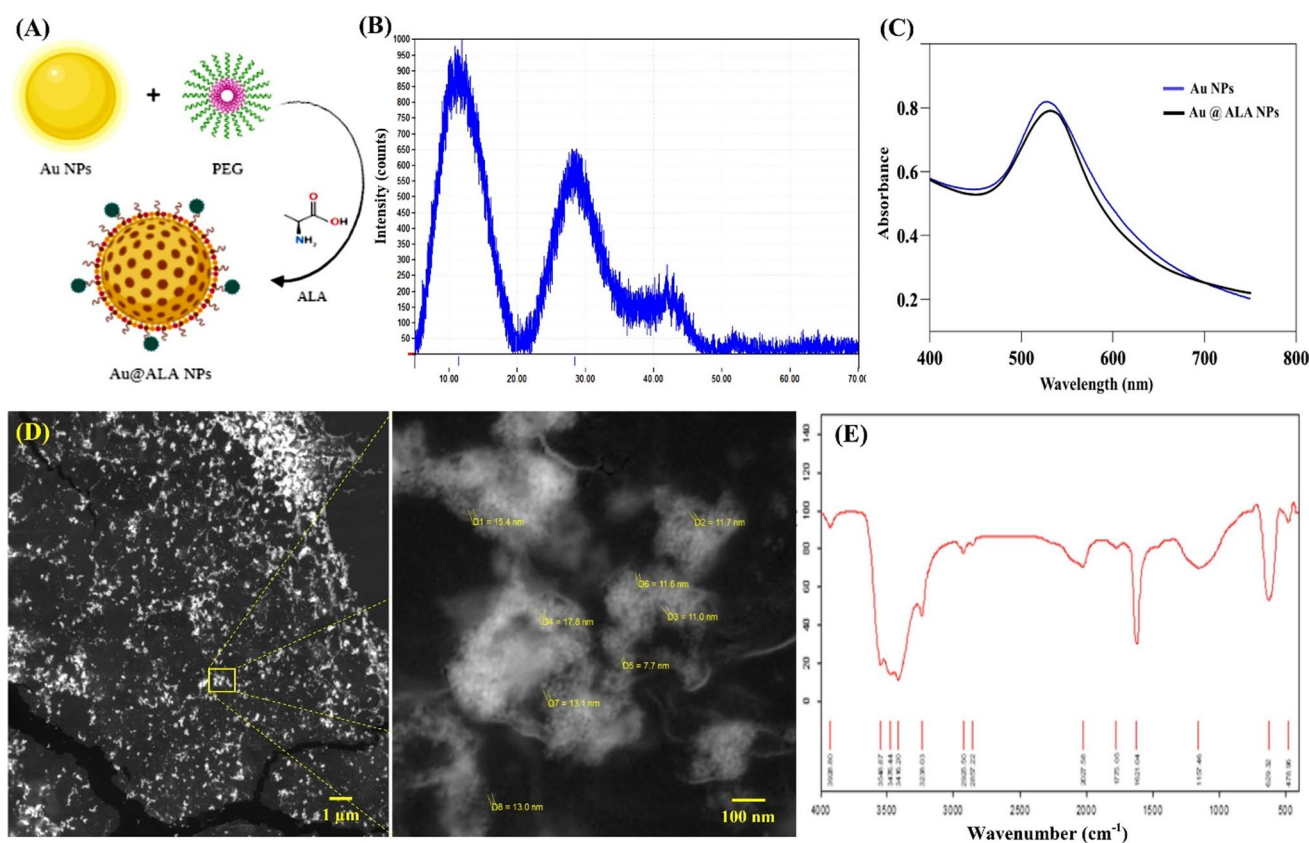


Fig. 1 Characterization of Au@ALA NPs. **A** Schematic illustration showing the synthesis of PEGylated-Au@ALA NPs for breast cancer radio-photo dynamic therapy, **B** Diffraction (XRD) analysis of Au NPs, **C** ultraviolet–visible (UV–Vis) spectroscopy of the Au

NPs and PEGylated-Au@ALA NPs, **D** transmission electron microscope (TEM) images of the Au@ALA NPs with different scales, and **E** Fourier transform infrared (FTIR) spectra of Au@ALA NPs. Gold nanoparticles (Au NPs)

peaks consistent with the standard Bragg reflections (111), (200), (220), and (311), indicating a face-centered cubic lattice structure. In Fig. 1C, the UV–visible spectra of pure Au NPs and PEGylated-Au@ALA NPs are presented. The characteristic surface Plasmon resonance (SPR) peak of Au NPs is observed around 525 nm. After the PEG-ALA coating, a slight red shift is observed in the UV–visible spectrum, with the maximum absorption peak shifting to approximately 521 nm. This redshift is accompanied by an increase in the peak intensity. The results indicate that the surface modification of Au@ALA NPs with PEG-ALA does not significantly alter their morphology and optical properties. Also, the position of the SPR peak is prejudiced by the physical size of the NPs, and a decrease in size can lead to a shift in the peak wavelength.

Also, Fig. 1D displays a TEM micrograph and size distribution of Au@ALA NPs. TEM was performed to assess the morphological characteristics of Au@ALA NPs. The TEM micrographs confirm that all the particles are nearly sphere-shaped with a fairly narrow size distribution of 10–30 nm. Moreover, the FTIR spectra of Au@ALA NPs are presented in Fig. 1E. It showed that the peaks at 3416 cm^{-1} , 1621 cm^{-1} , and 623 cm^{-1} corresponded to bonded amide (–NH–) stretching vibrations, which further approved the effective conjugation of PEGylated-Au@ALA NPs surface [27].

3.2 In-vitro cytotoxicity assay

To examine the cytotoxicity of synthesized NPs on two cancerous and healthy cell lines of the Breast (MCF-7 and MCF-10), the cytotoxicity assay was carried out in the existence of various concentrations of Au@ALA NPs. The cell viability of MCF-10 and MCF-7 cell lines using diverse concentrations of Au@ALA NPs is shown in Fig. 2. For

treated MCF-10 cells with concentrations of 6.25, 12.5, 25, 50, 100, 150, and 200 $\mu\text{g/ml}$ Au@ALA NPs, cell viabilities were 97.83%, 95.95%, 93.12%, 90.12%, 87.97%, 84.90%, and 83.05%, respectively, in contrast to 100% in the absence of NPs. Similarly, cell viabilities for the same concentration of Au@ALA NPs for MCF-7 cells were 93.00%, 86.07%, 80.87%, 77.93%, 75.17%, 72.04%, and 67.94%, respectively. Therefore, Fig. 2 disclosed the influence of different concentrations of Au@ALA NPs on cell damage. It was clear that the swelling concentration of NPs from 6.25 to 200 $\mu\text{g/ml}$, attributed to reducing the cell viabilities from 97.83% to 83.05% (about 14% reduction) for MCF-10 cells ($P > 0.05$). For treated MCF-7 cells with NPs, this reduction was from 93.00% to 67.94% at the same concentrations, respectively (an approximately 26% decline) ($P > 0.05$). Consequently, it was found that the cancerous MCF-7 cells were more susceptible than healthy MCF-10 cell lines. Similarly, in all single concentrations, the cell survival rate in the MCF-10 cell line was higher than in the MCF-7 cell line. This high sensitivity can be due to the difference in the nature and characteristics of cancerous tissue from healthy tissue. The results are consistent with similar cytotoxicity studies. Moses et al. investigated the cytotoxicity of Au NPs in MCF-7 and MDA-MB-231 BC cells and normal MCF-10 breast cell lines. The results of the apoptosis analysis showed that considerable apoptosis did not occur in MCF-10 cells, while MDA-MB-231 and MCF-7 cells showed the formation of apoptotic bodies, especially in concentrations of Au NPs that exceeded the determined IC₅₀ values [28].

Fig. 2 Cell viability results of different concentrations of Au@ALA NPs on both MCF-7 and MCF-10 cell lines. Gold nanoparticles (Au NPs)

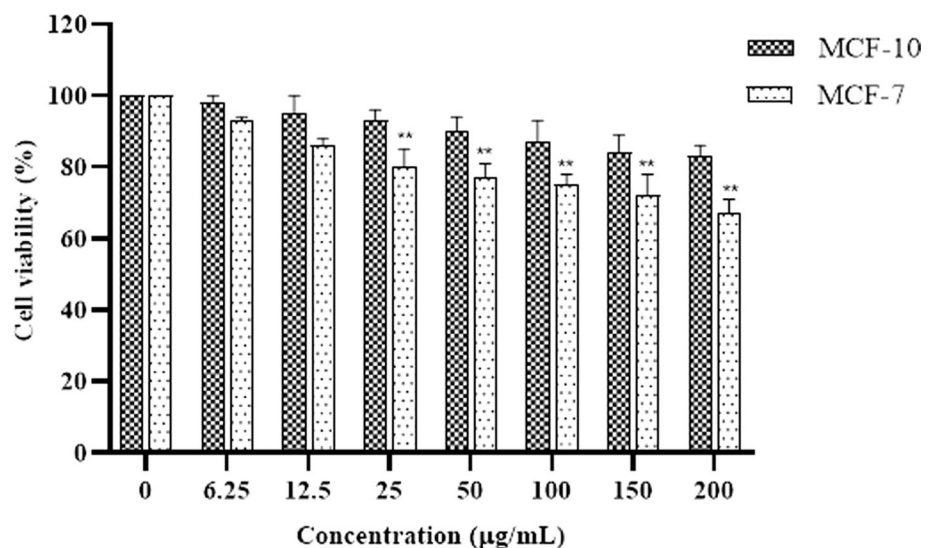
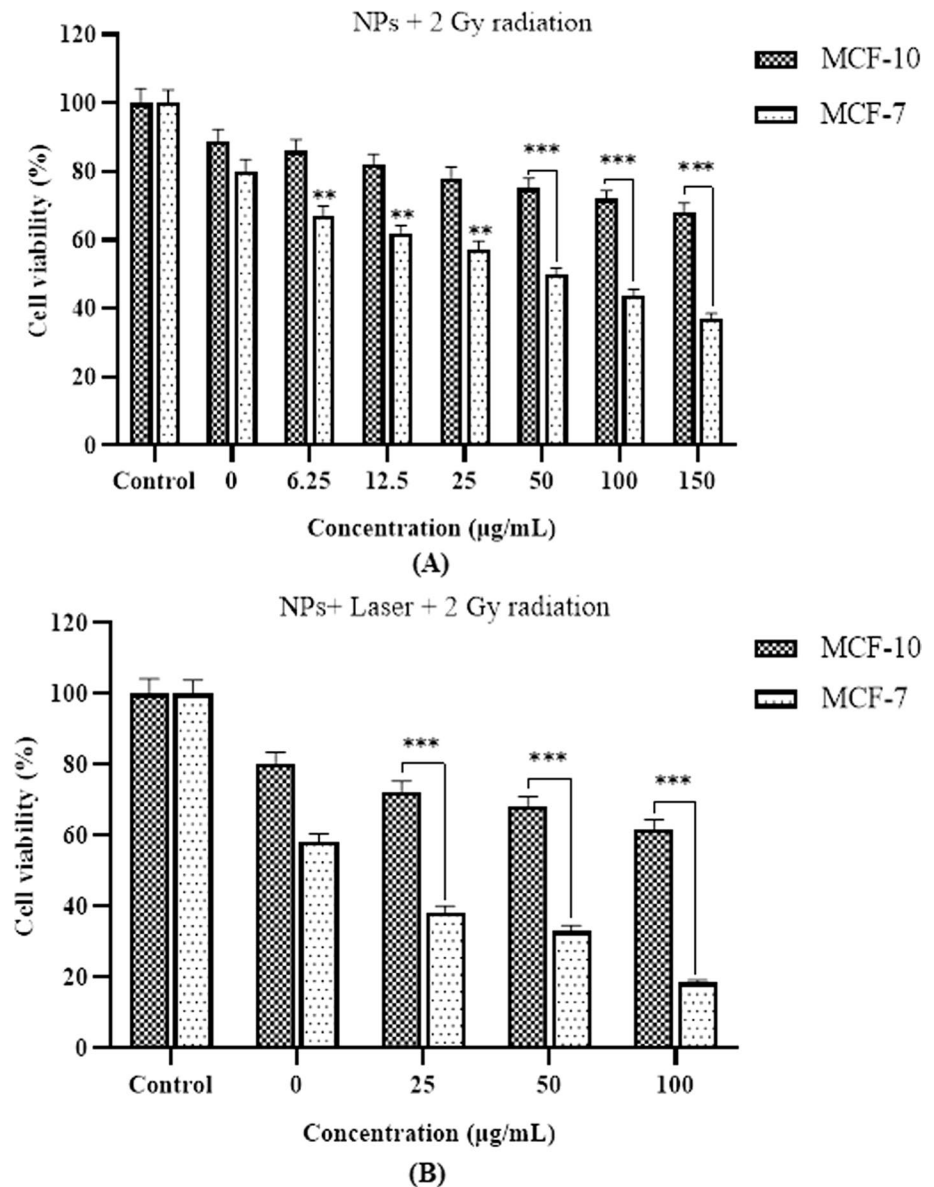


Fig. 3 Cell viability results of different concentrations of **A** Au@ALA NPs and 2 Gy dose; **B** photodynamic therapy + Au@ALA NPs on both MCF-7 and MCF-10 cell lines after exposure to 2 Gy dose. Gold nanoparticles (Au NPs)



3.3 Photodynamic therapy and radiosensitization effects of Au@ALA NPs

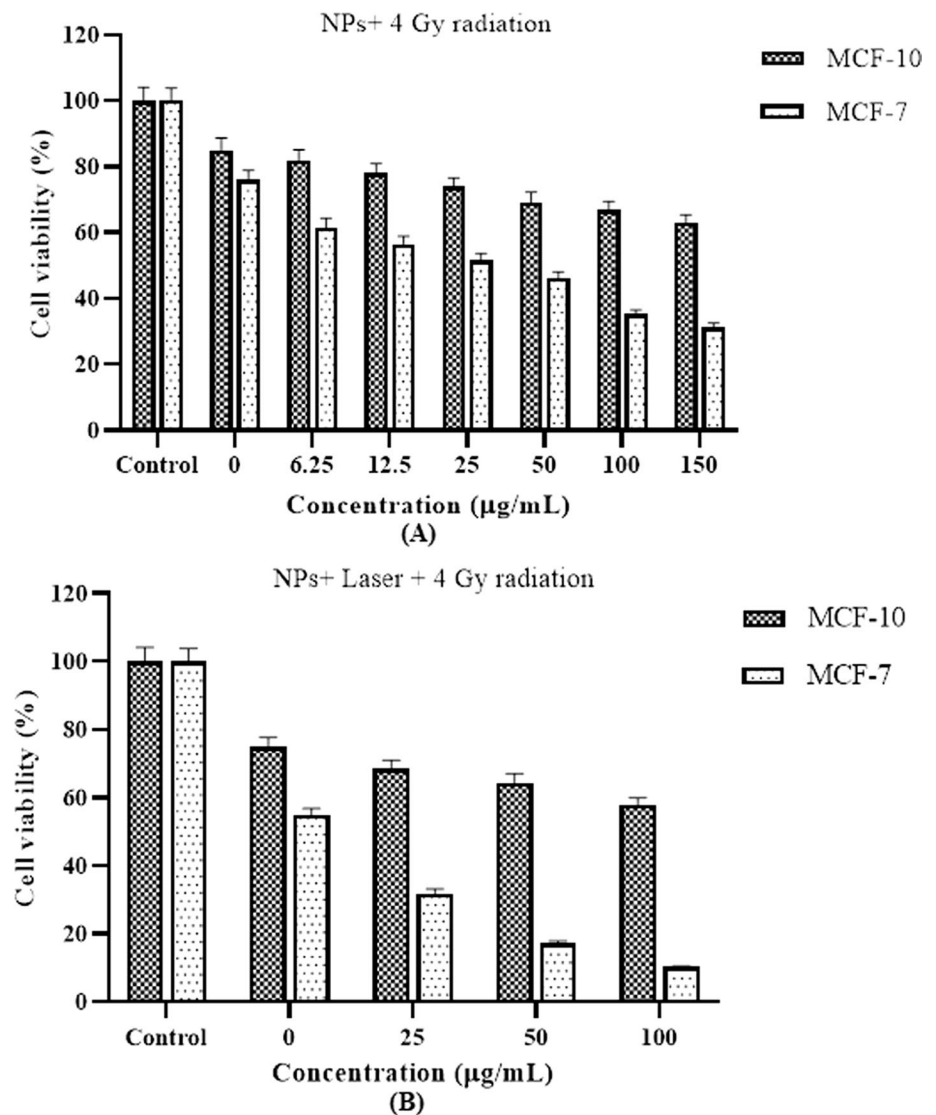
The cell viability of MCF-10 and MCF-7 cell lines by varied concentrations of Au@ALA NPs in the presence of 6 MV (2 Gy) radiation with and without laser is shown in Fig. 3.

The cell viabilities of treated MCF-10 cells with concentrations of 0, 6.25, 12.5, 25, 50, 100, and 150 µg/ml Au@ALA NPs were 88.87%, 85.98%, 82.11%, 78.02%, 75.00%, 71.90%, and 68.14%, respectively under 2 Gy radiation. As well, cell viabilities for 0, 6.25, 12.5, 25, 50, 100, and 150 µg/ml NPs concentrations for MCF-7 cells were observed 79.95%, 67.08%, 62.02%, 57.13%, 49.89%, 43.89%, and 36.99%, respectively, under 2 Gy radiation (Fig. 3A). Moreover, Fig. 3B portrays sustainability of the both cells for 0, 25, 50, and 100 µg/ml NPs' concentrations following

the radiation dose of the 2 Gy + laser group. Also, the cell viabilities were 80.07%, 72.02%, 68.20%, and 61.66%, respectively for MCF-10 and 58.00%, 38.25%, 32.99%, and 18.37%, respectively, for MCF-7 cell line. It was found that without using radiation, the cell viability of both cell lines witnessed a reduction trend; at first, they were 87.97% and 75.17 for MCF-10 and MCF-7, respectively; after applying 6 MV radiation 2 Gy, the cell viabilities decreased to 88.87% and 79.95%, respectively.

Similarly, cell viabilities for 0, 6.25, 12.5, 25, 50, 100, and 150 µg/ml NPs concentrations for MCF-10 cells were observed at 84.94%, 81.81%, 77.97%, 73.98%, 69.15%, 66.81%, and 63.05%, respectively, under 4 Gy radiation. These numbers for MCF-7 cells were 75.93%, 61.58%, 56.53%, 51.53%, 46.23%, 35.25%, and 31.24%, respectively (Fig. 4A). These numbers for cells treated with 0, 25, 50, and

Fig. 4 Cell viability results of different concentrations of **A** Au@ALA NPs and **B** photodynamic therapy + Au@ALA NPs on both MCF-7 and MCF-10 cell lines after exposure to 6 MV with 4 Gy dose radiation. Gold nanoparticles (Au NPs)



100 µg/ml NPs concentrations + 4 Gy radiation + laser group were 74.81%, 68.35%, 64.24%, and 57.88%, respectively for MCF-10 and 54.82%, 31.67%, 17.18%, and 10.10%, respectively, for MCF-7 cell line (Fig. 4B).

It was found that in the presence of a 2 Gy dose of 6 MV X-ray radiation and without using NPs, the cell viability was 88.87% and 79.95 for MCF-10 and MCF-7, respectively. While at 100 µg/ml NPs concentrations, the cell viabilities decreased to 71.90% and 43.89%, respectively. First, it is clear that MCF-7 cells were more susceptible than MCF-10. Also, comparing Fig. 3B and Fig. 4B, it is revealed that at the same energy, increased radiation dose related to further cellular injury and the highest extent of cell harm happened at 4 Gy. These results are following the results of studies in which an enlarged apoptosis rate has been found when NPs were used for BC cell cure.

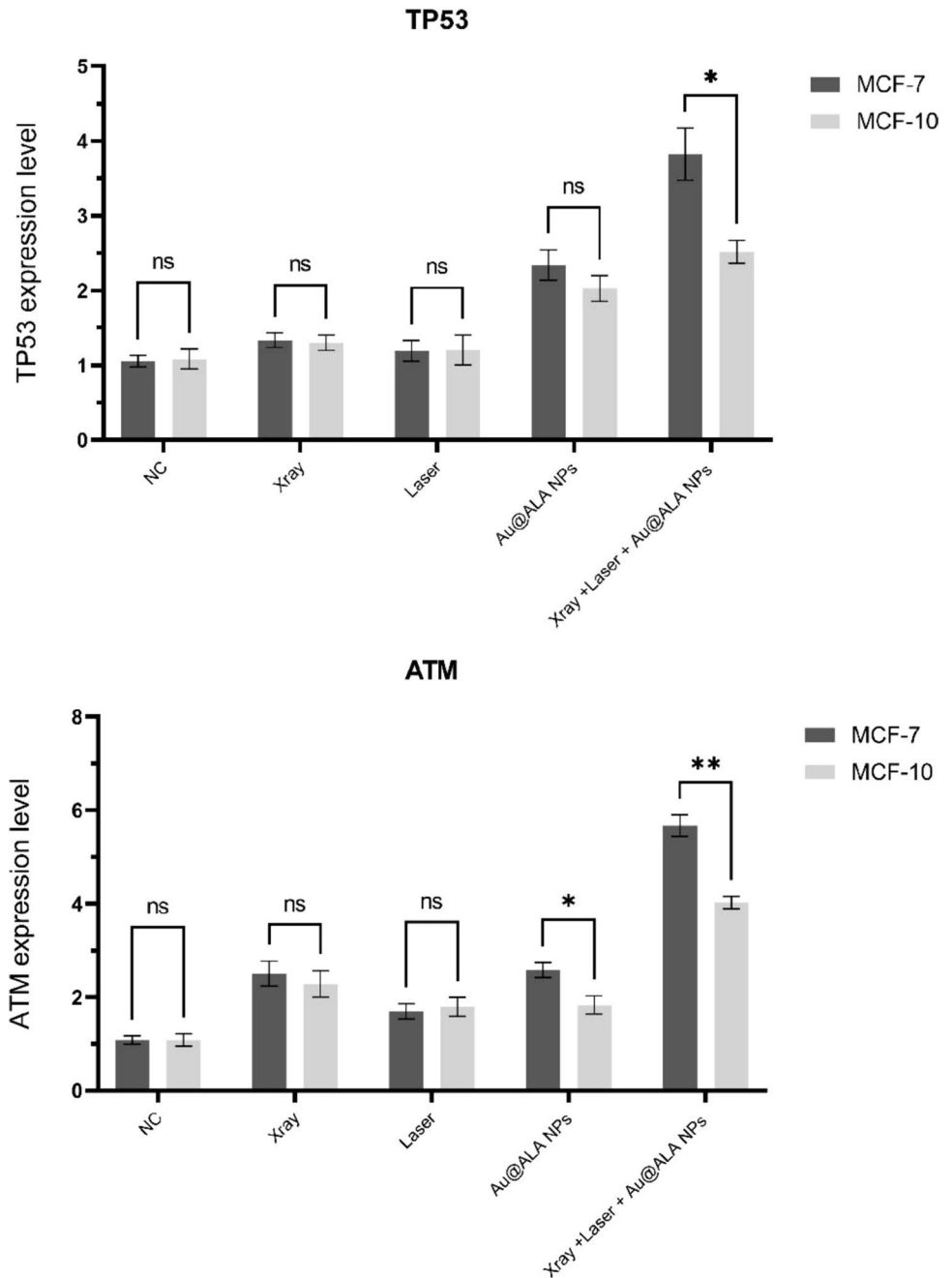
From the results (Fig. 4A), it is obvious that cellular damage increases as the radiation dose increases. The cell

viability for concentration 100 µg/ml NPs was 43.69% in contrast to 79% in the lack of NPs at similar radiation energy and absorbed dose.

3.4 The expression level of TP53 and ATM genes

To evaluate the expression of TP53 and ATM genes which participate in the DNA damage response, the qRT-PCR was performed. The result showed that the expression levels of both genes increased significantly in the X-ray + Laser + Au@ALA NPs exposed group in the MCF-7 cell line compared to the MCF-10 cell line. Also, the expression level of the ATM gene was significantly increased in the Au@ALA NPs treated group in the MCF-7 cell line compared to the MCF-10 cell line which indicates the intensity of DNA damage response in the cancerous cell line compared to the normal cell line (Fig. 5).

Fig. 5 Expression level of TP53 and ATM genes in both MCF-7 and MCF-10 cells treated with Au@ALA nanoparticles (NPs), laser radiation, X-ray radiation (6 MV with 4 Gy), and NPs + Laser + X-ray radiation



3.5 Colony formation of MCF-10 cells

To evaluate the effects of radio-sensitizing ability of combination therapy, we examined the proliferation ability of the MCF-10 cell line by CFA after applying Au@ALA NPs, laser radiation, X-ray radiation (6 MV with 4 Gy), and X-ray + Laser + Au@ALA NPs treatment. As shown in Fig. 6, in the case of combination therapy, the colony formation was decreased compared to other groups. Hence, our results showed that the combination of X-ray + Laser + Au@

ALA NPs reduced the capacity of the cells to grow into colonies.

4 Discussion

Numerous educations have demonstrated noteworthy variations in the repair of sub-lethal damage among diverse cell lines [29]. In line with this, Darfarin et al. investigated the radiosensitization potential of Au@Si₂O core-shell NPs on the MCF-7 cell line using 6 and 18 MV (2, 4, and 8 Gy).

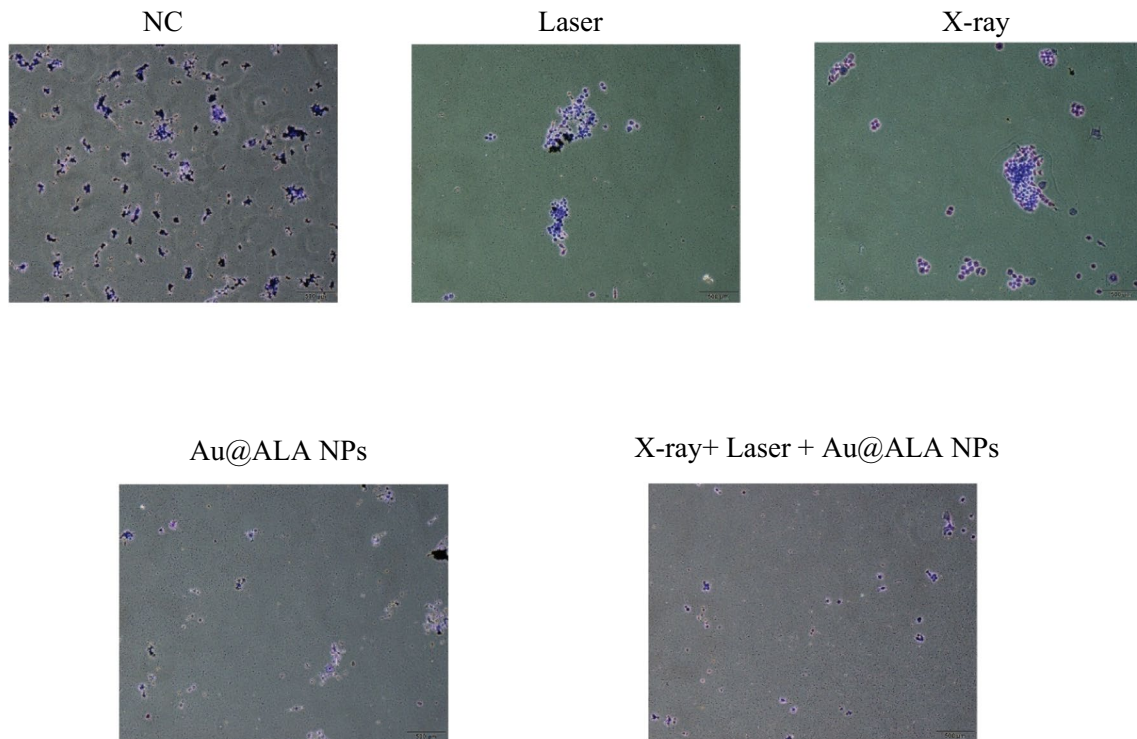
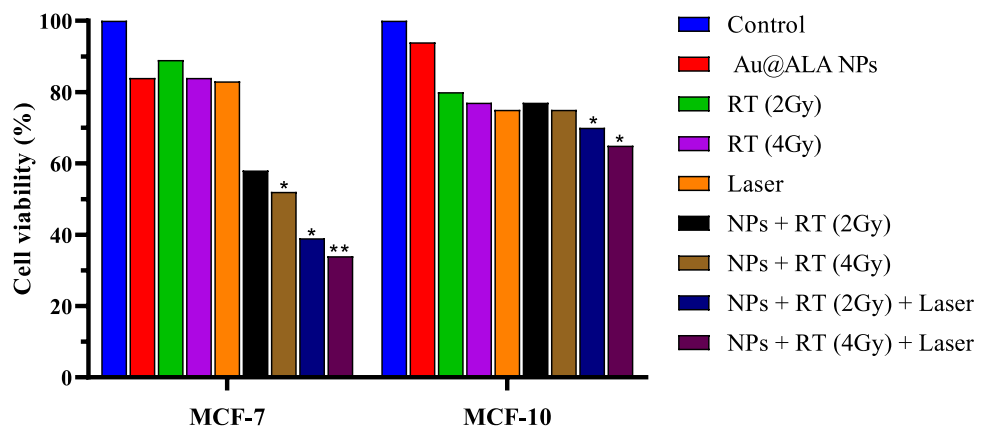


Fig. 6 Colony formation images of MCF-7 cells treated with Au@ALA nanoparticles (NPs), laser radiation, X-ray radiation (6 MV with 4 Gy), and NPs + Laser + X-ray radiation

Fig. 7 Cell viability results of Au@ALA NPs (25 µg/ml), X-ray radiation (RT, 6 MV), laser, and all combination groups on both MCF-7 and MCF-10 cell lines



They observed that, at a consistent absorbed dose, the radiation dose improvement achieved with 18 MV was greater compared to that with 6 MV [30].

According to Fig. 7., it is evident that the combination of targeted Au@ALA NPs with a radiation dose of 4 Gy in 6 MV + laser radiation induces advanced cytotoxicity in both cell lines compared to the groups treated with NPs or radiation alone at similar concentrations and radiation doses ($P < 0.05$). These results demonstrate that the synergistic effect of targeted Au@ALA NPs, radiation, and laser treatment leads to increased tumor cell death associated with the untreated groups. The remarkable accumulation

of tumor-targeted Au@ALA NPs in cancer cells highlights their significant potential in nano-medicine with broad clinical applications.

Indeed, similar findings have been reported by Darfarin et al. in their research, who investigated the use of amine and thiol-activated core-shell NPs (AuN@SiO_2 ; AuS@SiO_2) as RS. Their results showed a growth in the amount of cells in the G0-G1 phase. The cell cycle response was found to depend on the cell type and dose rate, with some cell lines exhibiting a dose edge below which they do not respond to radiation [30]. The simultaneous use of NPs, radiation therapy, and laser further enhances the cytotoxic effects on

both MCF-7 and MCF-10 cells. Additionally, the results indicate maximum cytotoxic potential at a radiation dose of 4 Gy. Furthermore, it was confirmed that NPs exhibit toxicity even in the lack of radiation.

Heinfeld et al. described the ability of 1.9 nm Au NPs to regulate the progression of BC using 250 kVp radiation (30 Gy), resulting in a 1 year survival rate of approximately 87% compared to around 20% with X-rays alone [31]. Similarly, Rahman et al. examined the radiation dose boost of various concentrations of 1.9 nm Au NPs on BAE cells. They observed a significant increase in the dose enhancement factor (DEF) with higher NP concentrations. DEFs of 25 and 4 were reported when using 1 mM and 0.25 mM concentrations at 80 kVp in turn [14]. However, Jain et al. assessed the collective cytotoxicity of 1.9 nm Au NPs with 160 kVp radiation and found an average DEF of 1.4 in MDA-MB-231 BC cells. Furthermore, Butterworth et al. examined the radiation improvement of Au NPs in various cell lines using two dissimilar concentrations at a radiation energy of 160 kVp. They observed variable DEFs for different cell lines, with values of 0.86 and 0.87 for the L132 cell line, 1.16 and 1.97 for the AGO cell line, and 1.30 and 1.91 for the T98G cell line, using 0.05 mM and 0.5 mM Au NP concentrations, respectively [32].

The diverse results obtained from these studies raise several important questions, including the necessity of achieving intracellular delivery of NPs for improved radiation dose enhancement. It is known that NPs initially accumulate in cancer cells due to their leaky vasculature, permeation, and retention (EPR) effect [33]. Recently, the impact of glucose-covered Au NPs (Glu-Au NPs) on MCF-7 cells under Kevrange radiation was evaluated. It was observed that while non-targeted Au NPs were mostly confined to the cell membrane, Glu-Au NPs entered the cells and distributed within the cytoplasm. Interestingly, Glu-Au NPs-induced higher levels of cell death compared to non-targeted Au NPs, suggesting that internalization is crucial for enhancing the radiation dose of the NPs [34].

Moreover, a study demonstrated that DNA injury in cells treated with Trastuzumab (TZ)-PEG-Au NPs was approximately 5 and three times greater than in cells treated with PEG-Au NPs and control cells, in turn. The surface reform of Au NPs with TZ enabled their binding to HER-2 expressing cells, facilitating their entry into the cell cytoplasm through the EPR process. This led to significant DNA damage through biochemical and biophysical mechanisms [35].

Studies have shown more extensive delays in the G₂ phase of the cell cycle when cells are exposed to high-LET (linear energy transfer) radiation up to 300 keV/μm, compared to X-ray exposure. This suggests that high-LET radiation can induce more pronounced cell cycle arrests at the G₂ checkpoint, mediated in part by tumor suppressor protein p53 (TP53) signaling pathways. Furthermore, experiments

on human fibroblasts demonstrated clear differences in the cellular responses between wild-type and TP53 mutant cells following X-irradiation [36]. These findings underscore the important role that TP53 protein play in modulating the cellular response to varying qualities of ionizing radiation. Therefore, the TP53 plays a central role in coordinating the cellular response to DNA damage. When DNA damage occurs, it triggers the activation of the ATM kinase protein, which act as sensors of the DNA lesions. Once activated, ATM phosphorylate and stabilize the p53 protein, causing it to accumulate in the cell nucleus. This phosphorylation event is a critical step that allows p53 to become transcriptionally active. Active p53 then goes on to regulate the expression of genes involved in cell cycle arrest, DNA repair processes, and apoptosis if the damage is too severe for the cell to recover [37]. Wan et al. and Prasad et al. have both explored the impacts of exposure to metal-based NPs on DNA damage response pathways in human cells. Wan et al. investigated the effects of Cobalt NPs on human lung epithelial cells, finding that Cobalt NPs exposure increased phosphorylation of the ATM protein, suggesting a role for oxidative stress and ATM activation in Cobalt NPs-induced DNA damage [38]. Similarly, Prasad et al. examined the effects of TiO₂ NPs on human dermal fibroblasts, and their results showed that TiO₂ NPs exposure led to activation of the ATM-mediated DNA damage response pathway in these cells [39]. Importantly, these results are consistent with our findings, further indicating that metal-based NPs have the ability to trigger ATM-dependent cellular mechanisms that detect and respond to DNA damage. In next experiments, the CFA results indicate a synergistic effect when using Au@ALA NPs in combination with either laser or X-ray radiation. Specifically, the data showed that adding the Au@ALA NPs to cells prior to irradiation (with either laser or X-ray) led to a decreased number of proliferating, colony forming cells compared to radiation exposure alone. This suggests that the combination of Au@ALA NPs and radiation results in increased cell apoptosis, rather than just cell proliferation. Additionally, the results showed a lower number of cellular foci (an indicator of DNA damage) in the cells exposed to the combined treatment of Au@ALA NPs and radiation, versus radiation alone. Taken together, these findings indicate a synergistic or enhanced effect when using the Au@ALA NPs in combination with radiotherapy, potentially leading to improved therapeutic outcomes compared to radiation treatment alone.

In the context of radiation at MV energy range, where Compton scattering and pair production dominate (particularly above 5 MeV), scattered photons and secondary electrons deposit most of their energy in the vicinity. In a similar vein, Babaei et al. investigated the impact of Fe₃O₄@Au NPs (25 nm) on the radiosensitivity of SKBr-3 BC cells during radiotherapy. SKBr-3 cells were treated with varying

concentrations of Fe₃O₄@Au NPs and exposed to radiation doses of 2, 4, and 8 Gy (6 and 18 MV). The results demonstrated that the cytotoxic effects increased with increasing NPs concentration and radiation dose in all the studied groups [13].

Evaluation of cell viability of MCF-7 BC cells, which include Au@ALA NPs and exposed to 6 MV (2 and 4 Gy) radiation and 640 nm laser radiation, indicated that simultaneous use of Au@ALA NPs was compulsory to decline significantly cell viability. The presented targeted radiosensitizer in the present study could be used to treat other tumor cells. Regardless of all the struggles and originations presented, the in vivo study of this suggestion appears actually fascinating, which the authors hope to address in future education.

5 Conclusions

This study focused on the development of Au@ALA NPs as potential radiosensitizers and radiation-enhancing agents for the treatment of breast cancer (BC) cells using MV radiation and photodynamic therapy (PDT). The Au@ALA NPs exhibited selective damage to cancer cells while sparing normal tissue. Moreover, when combined with 2 and 4 Gy doses of MV radiation, these NPs demonstrated significant radio-sensitizing effects, particularly at the higher dose of 4 Gy. The results indicated a synergistic effect when the targeted NPs, PDT, and radiation therapy were combined. These findings have implications for future cancer treatment strategies, highlighting the potential of bio-radiosensitizers in combination with MV radiation and PDT.

Acknowledgements This work is extracted from a Ph.D. thesis in the Nuclear Engineering Department by Omid Talaei and supported by the Vice-Chancellery of Research, Shiraz University.

Author contributions OT: data curation; formal analysis; investigation; writing—original draft, RF: funding acquisition; project administration; resources; supervision; validation; visualization; review and editing, BR: conceptualization, formal analysis; methodology; review and editing, SS: methodology; review & editing.

Funding This research did not receive any specific grant from funding agencies in the public, commercial, or not-for-profit sectors.

Declarations

Conflict of interest None of the authors have any conflicting interests.

Ethical approval This article does not contain any studies with human participants performed.

References

- Mandrik O, Zielonke N, Meheus F, Hans Severens JL, Guha N, Acosta RH, Murillo R. Systematic reviews as a 'lens of evidence': determinants of benefits and harms of breast cancer screening. *Int J Cancer*. 2019;145(4):994–1006. <https://doi.org/10.1002/ijc.32211>.
- Soni A, Ren Zh, Hameed O, Chanda D, Morgan ChJ, Siegal GP, et al. Breast cancer subtypes predispose the site of distant metastases. *Am J Clin Pathol*. 2015;143(4):471–8. <https://doi.org/10.1309/AJCPYO5FSV3UPEXS>.
- Collaborative Group on Hormonal Factors in Breast Cancer. Menarche, menopause, and breast cancer risk: individual participant meta-analysis, including 118 964 women with breast cancer from 117 epidemiological studies. *Lancet Oncol*. 2012;13(11):1141–51. [https://doi.org/10.1016/S1470-2045\(12\)70425-4](https://doi.org/10.1016/S1470-2045(12)70425-4).
- Elahi N, Kamali M, Baghersad MH. Recent biomedical applications of gold nanoparticles: a review. *Talanta*. 2018;184:537–56. <https://doi.org/10.1016/j.talanta.2018.02.088>.
- Malekzadeh R, Babaye Abdollahi B, Ghorbani M, Pirayesh Islamian J, Mortezaazadeh T. Trastuzumab conjugated PEG–Fe₃O₄@Au nanoparticle as an MRI biocompatible nano-contrast agent. *Int J Polym Mater Polym Biomater*. 2023;72(10):759–70. <https://doi.org/10.1080/00914037.2022.2058944>.
- Ziyae S, Malekzadeh R, Ghorbani M, Nasiri Motlagh B, Asghariazar V, Mortezaazadeh T. Preparation of MnO₂@ poly-(DMAEMA-co-IA)-conjugated methotrexate nano-complex for MRI and radiotherapy of breast cancer application. *Magn Reson Mater Phys, Biol Med*. 2023. <https://doi.org/10.1007/s10334-023-01091-1>.
- Castano AP, Demidova TN, Hamblin MR. Mechanisms in photodynamic therapy: part one—photosensitizers, photochemistry and cellular localization. *Photodiagnosis photodyn Ther*. 2004;1(4):279–93. [https://doi.org/10.1016/S1572-1000\(05\)00007-4](https://doi.org/10.1016/S1572-1000(05)00007-4).
- Malekzadeh R, Mortezaazadeh T, Abdulsahib WK, Hamblin MR, Mansoori B, Alsaikhan F, Zeng B. Nanoarchitecture-based photothermal ablation of cancer: a systematic review. *Environ Res*. 2023. <https://doi.org/10.1016/j.envres.2023.116526>.
- Canaveso G, Ancona A, Racca L, Canta M, Dumontel B, Barbaresco F, et al. Nanoparticle-assisted ultrasound: a special focus on sonodynamic therapy against cancer. *Chem Eng J*. 2018;340:155–72.
- Alipour B, Mortezaazadeh T, Abdulsahib WK, Arzhang A, Malekzadeh R, Farhood B. A systematic review of multimodal application of quantum dots in breast cancer diagnosis: effective parameters, status and future perspectives. *J Drug Deliv Sci Technol*. 2023. <https://doi.org/10.1016/j.jddst.2023.104682>.
- Ayyami Y, Dastgir M, Ghorbani M, Jangjoo AG, Pourfarshid A, Malekzadeh R, Mortezaazadeh T. Characterization and application of targeted MnO₂/CS@ALA-MTX nano-radiosensitizers for boosting X-ray radiotherapy of brain tumors. *Colloids Surf, A*. 2024;692:133975. <https://doi.org/10.2217/nnm.14.100>.
- Costley D, Mc Ewan C, Fowley C, McHale AP, Atchison J, Nomikou N, et al. Treating cancer with sonodynamic therapy: a review. *Int J Hyperth*. 2015;31(2):107–17. <https://doi.org/10.3109/02656736.2014.992484>.
- Abdollahi BB, Ghorbani M, Hamishekar H, Malekzadeh R, Fara-jollahi A. Synthesis and characterization of actively HER-2 Targeted Fe₃O₄@Au nanoparticles for molecular radiosensitization of breast cancer. *BioImpacts*. 2022. <https://doi.org/10.34172/bi.2022.23682>.
- Rahman WN, Corde S, Yagi N, Abdul Aziz SA, Annabell N, Geso M. Optimal energy for cell radiosensitivity enhancement by gold

- nanoparticles using synchrotron-based monoenergetic photon beams. *Int J Nanomed*. 2014;9:2459. <https://doi.org/10.2147/IJN.S59471>.
15. Mello RS, Callisen H, Winter J, Kagan AR, Norman A. Radiation dose enhancement in tumors with iodine. *Med phys*. 1983;10(1):75–8. <https://doi.org/10.1118/1.595378>.
 16. Chithrani DB, Jelveh S, Jalali F, van Prooijen M, Allen C, Bristow RB, et al. Gold nanoparticles as radiation sensitizers in cancer therapy. *Radiat Res*. 2010;173(6):719–28. <https://doi.org/10.1667/RR1984.1>.
 17. Vickers NJ. Animal communication: when i'm calling you, will you answer too? *Curr Biol*. 2017;27(14):713–5. <https://doi.org/10.1016/j.cub.2017.05.064>.
 18. Hamblin MR, Hasan T. Photodynamic therapy: a new antimicrobial approach to infectious disease? *Photochem Photobiol Sci*. 2004;3(5):436–50. <https://doi.org/10.1039/b311900a>.
 19. Dolmans DEJGJ, Fukumura D, Jain RK. Photodynamic therapy for cancer. *Nat Rev Cancer*. 2003;3(5):380–7. <https://doi.org/10.1038/nrc1071>.
 20. Wu J, Han H, Jin Q, Li Z, Li H, Ji J. Design and proof of programmed 5-aminolevulinic acid prodrug nanocarriers for targeted photodynamic cancer therapy. *ACS Appl Mater Interfaces*. 2017;9(17):14596–605. <https://doi.org/10.1021/acsami.6b15853>.
 21. Guo S, Sun X, Cheng J, Xu H, Dan J, Shen J, et al. Apoptosis of THP-1 macrophages induced by protoporphyrin IX-mediated sonodynamic therapy. *Int J Nanomed*. 2013;8:2239. <https://doi.org/10.2147/IJN.S43717>.
 22. Reinert M, Piffaretti D, Wilzbach M, Hauger C, Guckler R, Marchi F, et al. Quantitative modulation of PpIX fluorescence and improved glioma visualization. *Frontiers Surgery*. 2019;6:41. <https://doi.org/10.3389/fsurg.2019.00041>.
 23. Kennedy JC, Pottier RH, Pross DC. Photodynamic therapy with endogenous protoporphyrin IX: basic principles and present clinical experience. *J Photochem Photobiol B: Biol*. 1990;6(1–2):143–8. [https://doi.org/10.1016/1011-1344\(90\)85083-9](https://doi.org/10.1016/1011-1344(90)85083-9).
 24. Binkley JM, Harris SR, Levangie PK, Pearl M, Guglielmino J, Kraus V, et al. Patient perspectives on breast cancer treatment side effects and the prospective surveillance model for physical rehabilitation for women with breast cancer. *Cancer*. 2012;118(S8):2207–16. <https://doi.org/10.1002/cncr.27469>.
 25. Rosa S, Connolly C, Schettino G, Butterworth K, Prise KM. Biological mechanisms of gold nanoparticle radiosensitization. *Cancer Nanotechnol*. 2017;8(1):1–25. <https://doi.org/10.1186/s12645-017-0026-0>.
 26. Bentzen SM. Preventing or reducing late side effects of radiation therapy: radiobiology meets molecular pathology. *Nature Rev Cancer*. 2006;6(9):702–13. <https://doi.org/10.1038/nrc1950>.
 27. Abdelkader NF, El-Batal AI, Amin YM, Hawas AM, Hassan SH, Eid NI. Neuroprotective effect of gold nanoparticles and alpha-lipoic acid mixture against radiation-induced brain damage in rats. *Int J Mole Sci*. 2022;23(17):9640. <https://doi.org/10.3390/ijms23179640>.
 28. Moses SL, Edwards VM, Brantley E. Cytotoxicity in MCF-7 and MDA-MB-231 breast cancer cells, without harming MCF-10A healthy cells. *J Nanomed Nanotechnol*. 2016;7(369):2. <https://doi.org/10.4172/2157-7439.1000369>.
 29. Zhang J, Zhao T, Han F, Hu Y, Li Y. Photothermal and gene therapy combined with immunotherapy to gastric cancer by the gold nanoshell-based system. *J Nanobiotechnol*. 2019;17(1):1–11. <https://doi.org/10.1186/s12951-019-0515-x>.
 30. Darfarin G, Salehi R, Alizadeh E, Nasiri Motlagh B, Akbarzadeh A, Farajollahi A. The effect of SiO₂/Au core-shell nanoparticles on breast cancer cell's radiotherapy. *Art Cells, Nanomed Biotechnol*. 2018;46(2):836–46. <https://doi.org/10.1080/21691401.2018.1470526>.
 31. Hainfeld JF, Dilmanian FA, Zhong Z, Slatkin DN, Kalef-Ezra JA, Smilowitz HM. Gold nanoparticles enhance the radiation therapy of a murine squamous cell carcinoma. *Phys Med Biol*. 2010;55(11):3045. <https://doi.org/10.1088/0031-9155/55/11/004>.
 32. Jain S, Coulter JA, Hounsell AR, Butterworth K, McMahon SJ, Hyland WB, et al. Cell-specific radiosensitization by gold nanoparticles at megavoltage radiation energies. *Int J Radiat Oncol Biol Phys*. 2011;79(2):531–9. <https://doi.org/10.1016/j.ijrobp.2010.08.044>.
 33. Abdollahi BB, Malekzadeh R, Pournaghi Azar F, Salehnia F, Naseri AR, Ghorbani M, et al. Main approaches to enhance radiosensitization in cancer cells by nanoparticles: a systematic review. *Adv Pharmaceut Bulletin*. 2020;11(2):212–23. <https://doi.org/10.34172/apb.2021.025>.
 34. Kong T, Zeng J, Wang X, Yang X, Yang J, McQuarrie S, et al. Enhancement of radiation cytotoxicity in breast-cancer cells by localized attachment of gold nanoparticles. *Small*. 2008;4(9):1537–43. <https://doi.org/10.1002/sml.200700794>.
 35. Chattopadhyay N, Cai Z, Pignol JP, Keller B, Letchman E, Bendayan R, et al. Design and characterization of HER-2-targeted gold nanoparticles for enhanced X-radiation treatment of locally advanced breast cancer. *Mole Pharmaceut*. 2010;7(6):2194–206. <https://doi.org/10.1021/mp100207t>.
 36. Zhang Q, Kong Y, Yang Z, Liu Y, Liu R, Geng Y, Luo H, Zhang H, et al. Preliminary study on radiosensitivity to carbon ions in human breast cancer. *J Radiat Res*. 2020;1(3):399–409. <https://doi.org/10.1093/jrr/rraa017>.
 37. Haque M, Shakil MS, Mahmud KM. The promise of nanoparticles-based radiotherapy in cancer treatment. *Cancers*. 2023;15(6):1892. <https://doi.org/10.3390/cancers15061892>.
 38. Wan R, Mo Y, Feng L, Chien S, Tollerud DJ, Zhang Q. DNA damage caused by metal nanoparticles: involvement of oxidative stress and activation of ATM. *Chem Res Toxicol*. 2012;25(7):1402–11. <https://doi.org/10.1021/tx200513t>.
 39. Prasad RY, Chastain PD, Nikolaishvili-Feinberg N, Smeester L, Kaufmann WK, Fry RC. Titanium dioxide nanoparticles activate the ATM-Chk2 DNA damage response in human dermal fibroblasts. *Nanotoxicol*. 2013;7(6):1111–9. <https://doi.org/10.3109/17435390.2012.710659>.

Publisher's Note Springer Nature remains neutral with regard to jurisdictional claims in published maps and institutional affiliations.

Springer Nature or its licensor (e.g. a society or other partner) holds exclusive rights to this article under a publishing agreement with the author(s) or other rightsholder(s); author self-archiving of the accepted manuscript version of this article is solely governed by the terms of such publishing agreement and applicable law.